IJRCS
International Journal of Robotics and Control Systems
Vol. 4, No. 2, 2024, pp. 727-745
ISSN 2775-2658
http://pubs2.ascee.org/index.php/ijrcs
ASCEE

Bifurcation Analysis of a Non-Linear Vehicle Model Under Wet Surface Road Condition

Abhay Kumar [a,1], Suresh Kant Verma [a,2], Dharmendra Kumar Dheer [b,3,*]

[a] Department of Mechanical Engineering, National Institute of Technology Patna, India
[b] Department of Electrical Engineering, National Institute of Technology Patna, India
[1] abhayk.phd20.me@nitp.ac.in; [2] skverma@nitp.ac.in; [3] dkdheer@nitp.ac.in
[*] Corresponding Author

ARTICLE INFO

Article History
Received March 05, 2024
Revised April 07, 2024
Accepted May 16, 2024

Keywords
Nonlinear Vehicle Model;
Stability Analysis;
Phase Plane Method;
Hopf Bifurcation;
Saddle Node Bifurcation

ABSTRACT

The vehicles are prone to accidents during cornering on a wet or low friction coefficient roads if the longitudinal velocity (V_x) and steering angle (δ) are increased beyond a certain limit. Therefore, it is of major concern to analyze the behaviour and define the stability boundary of the vehicle for such scenarios. In this paper, stability analysis of a 2 degrees of freedom nonlinear bicycle model replicating a car model including lateral (sideslip angle β) and yaw (yaw rate r) dynamics only operating on a wet surface road has been performed. The stability is analysed by utilizing the phase plane method and bifurcation analysis. The obtained converging and diverging nature of the trajectories (β, r) depicts the stable and unstable equilibrium points in the phase plane. The movement of these points results in the transition of the stability known as bifurcation due to the change in the control parameters (V_x, δ). The Matcont/Matlab is utilized to obtain the bifurcation diagrams and the nature of bifurcations. The obtained results show that a saddle node (SNB) and a subcritical Hopf bifurcation (HB) exists for steering angle ($\pm$0.08 rad) and higher than ($\pm$0.08 rad) with V_x = (10 - 40) m/s respectively. The SNB and HB denotes the spinning of the vehicle and sliding of the vehicle respectively, thus generating a unstable behaviour. A stability boundary is obtained representing the stable and unstable range of parameters.

1. Introduction

Driving the vehicle on wet or low friction coefficient roads are dangerous, as the accidents are more frequent on these harsh road conditions. Due to the low friction coefficient, the vehicle does not experiences the required amount lateral force on tires to track the curvature of roads and thus resulting in lateral instability [1]. Lateral instability refers to the crossing of the vehicle states including yaw rate and sideslip angle beyond the defined stability limits. On the low friction roads, the sideslip angle increases beyond the stability limit resulting in the lateral slip of the vehicles. Bounding these state variables within the stability limits at low friction surface roads are therefore important to avoid accidents [2], [3]. The vehicle rapidly enters the nonlinear operating regions with sharp cornering on low friction surfaces. The nonlinear vehicle dynamics have a major impact on the vehicle stability. Consequently, consideration of the nonlinear characteristics is required on such low friction roads [4]. Therefore, to reflect the nonlinear characteristics, the Pacejka tire model is adopted in this paper. In [5], a 2 degrees of freedom model (bicycle model) is developed by assuming that the left and right tires

http://dx.doi.org/10.31763/ijrcs.v4i2.1346. ijrcs@ascee.org

are assumed to have similar behaviour and lumped to form single front and rear tires. The suspension movements, slip phenomena, and aerodynamic influences are neglected. The longitudinal velocity is assumed to be constant, therefore different values of velocity are opted for stability analysis.

The stability analysis of the nonlinear systems are observed with the help of phase plane and bifurcation methods [6]. The phase plane is a two dimensional instantaneous plot between two state variables of the system. The plane shows the trajectory of the state variables for specific values of system and input parameters. The plot will change with the change in these parameters. The convergence and divergence of the trajectories towards a point illustrates the existence of the stable and unstable equilibrium point or steady state respectively on the plane. The topological structure of the phase trajectories above will alter when a particular parameter is changed. For instance, a stable equilibrium point might have become unstable. It can be said that the system has undergone a bifurcation. Specifically, the system's stability will alter as its equilibrium point appears or disappears. A bifurcation is a qualitative shift in dynamics, and the bifurcation point is the corresponding parameter value of the bifurcation. Fork, Hopf, and saddle-node bifurcation are the three primary types of bifurcation [7]. A Hopf bifurcation (HB) is classified into two types as subcritical and supercritical. At a subcritical HB an unstable limit cycle exists prior to the bifurcation and forms the region of attraction of the stable equilibrium. The limit cycle shrinks and disappears at the bifurcation. At a supercritical HB a stable limit cycle emerges after the bifurcation. Trajectories initiating close to the unstable equilibrium exhibit oscillations with growing amplitude which are attracted by the limit cycle [8], [9]. A saddle-node bifurcation, tangential bifurcation, or fold bifurcation is a local bifurcation in which two fixed points (or equilibria) of a dynamical system collide and annihilate each other. The term "saddle-node bifurcation" is most often used in reference to continuous dynamical systems. In discrete dynamical systems, the same bifurcation is often instead called a fold bifurcation [10]. The position of saddle points changes resulting in change in the portraits of the phases as the parameters of interest changes including steering angle, longitudinal velocity and friction coefficient [11].

Phase plane analysis is one of the best methods for examining how control actions affect vehicle dynamics [12]. With the help of this analysis, it can said that whether the vehicle is stable or not in terms of lateral stability [13]. In [14], [15], authors have utilized the phase plane analysis to obtain the stability region of the vehicle. Regarding vehicle control, the authors in [16] determined the vehicle's stability domain boundary under various road adhesion coefficients and suggested that the degree of instability was determined by the distance between the unstable point and the stable boundary. Authors in [17], [18] have utilized the phase plane of sideslip angle, sideslip rate and yaw rate to define the stability region boundary of the 2 DOF vehicle model. Similarly, the two dimensional phase plane analysis method is used to determine the vehicle stability region, and the ideal state trajectory is always chosen to be the sideslip angle (β) and yaw rate r [19], [20]. In [21], authors have utilized a (β - r) phase plane to obtain a stability envelop for the control purpose. The equilibrium points are identified by the phase portrait approach, which also reveals the kind of instability present by the shifting of points and offers control recommendations to stabilise the shifting of these equilibria [22]. The stability region of the phase plane v_y-r is composed of the stable points in the dynamics of the system for the vehicle stability [23]. Authors in [24] provided a dissipation of the energy analysis approach and verified it in the (v_y-r) phase plane for vehicle plane motion stability analysis.

A subcritical Hopf bifurcation in the nonlinear system is interpreted if the perturbations are large, then the system will diverge away from stable equilibrium [25]. In [26], the dynamics of the vehicle models are studied using bifurcation analysis. Stable and unstable steady states are mapped out as a function of speed and steering angle. A lateral stability analysis is done on a non-linear vehicle model with the help of phase plane and bifurcation analysis to find the stable region based on the movements of equilibrium points. A 18 DOF unified dynamic model is developed to study the influence of braking on the vehicle driving stability considering the challenges of coupling of dynamics [27]. The study of bifurcation analysis of vehicles for the stability considering the coupling between the driving torque and steering angle is performed in [28]. In [29], authors have performed a bifurcation analysis control for a ship model maneuvering in a straight line with a proportional control. The vehicle stability is studied with the help of the movements of the equilibrium points locations on the phase portraits. The control parameters are chosen as longitudinal velocity and the steering angle [30]. Authors in [31], [32] have obtained a vehicle driving stability region between sideslip angle β and sideslip rate $\dot{\beta}$ for a nonlinear coupled dynamical system, utilizing bifurcation theory and phase plane analysis respectively for the controller design. In [33], authors have implemented bifurcation analysis on a traffic flow replicated by an artificial neural network car following model to avoid traffic jams. A comparative study is done between vehicle steering controller utilizing phase plane combined with bifurcation theory to obtain the driving stability region for lateral dynamics [34]. There are two types of bifurcation theory namely local and global. Properties near an equilibrium point or a periodic orbit are the subject of local bifurcations. Hopf bifurcation and the saddle node make up local bifurcation. It addresses the emergence of abrupt shifts from smooth, continuous parameter variations in the system response. It is assumed that these changes will happen gradually as long as the system's equilibrium is maintained. In general, abrupt large transients are not covered by this assumption [35]. Authors in [36] discusses the presence of Hopf bifurcation by analyzing the limit cycle behaviour in the nonlinear 2 DOF single track bicycle model. In [37], authors have utilized bifurcation theory for the 5 DOF nonlinear model to obtain the vehicle stability region.

Authors in [38], have obtained the stability region for state variables including sideslip angle, yaw rate based on the vehicle parameters for the purpose of controller design with the control input parameter chosen as the steering angle.A collision avoidance control system is implemented based on a 2 DOF nonlinear bicycle model considering the slippery. The yaw rate constraint considering side-slip angles is utilized to prevent the vehicle from becoming unstable on slippery roads [39].

Based on the literature review it is found that the phase plane analysis and bifurcation analysis are the tools for analyzing the stability of the nonlinear vehicle model. A 2 DOF nonlinear vehicle bicycle model is sufficient to replicate the lateral dynamics. Following are the areas of research gaps are yet unexplored for the observing the vehicle lateral stability found:

- There are many nonlinear vehicle models proposed considering different dynamical equations. Nevertheless, for the control and stability of a nonlinear vehicle model, the bifurcation analysis work done is limited to linear and limited nonlinear models.
- The transition of stability of the vehicle models is analyzed for lower values of the control parameter. Generally, the value of the steering angle opted for is up to (± 0.08 rad). For lower values, the vehicle models depict a simple saddle node bifurcation. The stability region for this bifurcation does not focus on higher values of control parameters.
- Higher values of the control parameters for stability analysis are ignored to avoid the complexity of finding the nature of bifurcation near the stability boundary inside the stability region.

Based on the found research gaps, authors have contributed the field of research with the following works:

- To analyze the stability, a 2 DOF nonlinear vehicle informative model is utilized from the literature for stability analysis. The phase plane and bifurcation method are implemented in this model to find out the region of stability.
- To find out the type of bifurcation that exists for a higher value of steering angle and longitudinal velocity, the value is increased beyond (± 0.08 rad) and 20 m/s and thus the stability of the vehicle is analyzed for the design of the controller constraints.
- For higher values of the control input parameters (V_x, δ), the nature of bifurcation near the stability boundary is analyzed.

This paper primarily focuses on the stability analysis of the lateral dynamics of the nonlinear vehicle on the wet road conditions. The lateral dynamics of the vehicle include sideslip angle and

Vol. 4, No. 2, 2024, pp. 727-745

the yaw rate of the vehicle. Therefore, in this paper, a 2 degrees of freedom (DOF) nonlinear vehicle model also known as bicycle model is adopted for the purpose of stability analysis. This model is the simplified form of a vehicle model to replicate the lateral dynamics. Phase plane analysis is performed on the lateral dynamics to observe the trajectories of sideslip angle and yaw rate based on the change in the input parameters. The steering angle and longitudinal velocity are chosen as input parameters as these are most prominent parameters utilized. Since the lateral dynamics does not include longitudinal, vertical and wheel dynamics, therefore the results are limited to change in the trajectories of yaw rate and sideslip angle. Bifurcation method is utilized to observe the type of bifurcation exists for the change in bifurcation parameters (input parameters). Further, the article is organized as follows: Section 1 deals with the mathematical model of the nonlinear vehicle. Equilibrium point and bifurcation theory is described in the Section 2. Section 3 is the simulation results and discussion. Finally the conclusion is provided in the Section 4.

2. Method

This section discusses about the nonlinear mathematical vehicle model and the stability analysis. For this analysis, the phase plane and bifurcation theory is exploited.

2.1. Mathematical Modelling

In this paper, a bicycle dynamic model as shown in Fig. 1 is utilized because it is mathematically the simplest form to describe the dynamic characteristics of vehicles, it is shown to be sufficiently accurate for vehicle behaviour. The assumption [5] are included while developing the mathematical model. This model depicts the yaw rate and sidelsip angle as the lateral dynamics. As this model includes only dynamic variables therefore it is easier to analyse the stability and to design the controller. Including different other dynamics such as longitudinal, roll and wheel dynamics will increase degrees of freedom and thus mathematical complexity of model [40].

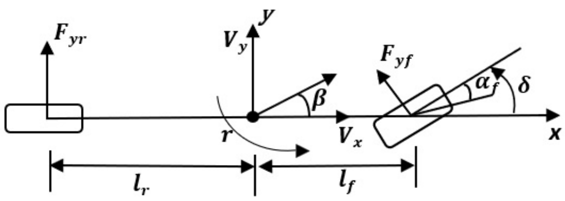

Fig. 1. Vehicle bicycle model

The general nonlinear differential equation is represented in (1) as:

$$\dot{\hat{x}} = f(\hat{x}, u) \tag{1}$$

where, $\hat{x} = [x_1 x_2 .. x_n]'$, n is the number of states. For the model adopted for the stability analysis, states are defined as $x_1 = \beta, x_2 = r$.

A 2 DOF nonlinear bicycle vehicle mathematical model [41] is adopted in this paper for its bifurcation analysis is described in (2):

$$(\beta, r) = f(F_{yf}, F_{yr}) \tag{2}$$

where, β is the vehicle sideslip angle, r is the yaw rate, $F_{y,i}$ represents the front F_{yf} and the rear F_{yr} lateral tire forces. The single track bicycle model [42] for vehicle body frame is described in (3) and (4):

$$\sum F_y = mV_x(\dot{\beta} + r) = F_{yf}cos(\delta) + F_{yr} \tag{3}$$

$$\sum M_z = I_z\dot{r} = l_fF_{yf}cos(\delta) - l_rF_{yr} \tag{4}$$

where, m is the mass of the vehicle, V_x is the longitudinal velocity at centre of gravity (CG), δ is the steering angle, I_z is the yaw moment of inertia, l_f is the distance between the front axle and CG, l_r is the distance between the rear axle and CG. The front and rear tire forces are given by Magic formula described in (5) as:

$$F_{y,i} = \mu D sin\{C tan^{-1}[B\alpha_i - E(B\alpha_i - tan^{-1}(B\alpha_i))]\} \tag{5}$$

where, μ is the friction coefficient and B, C, D, E are the tire coefficients obtained from [34] and the values are shown in Table 1. α_f and α_r are the front and rear tire slip angles defined by the (6) and (7):

$$\alpha_f = \beta + \frac{l_f r}{V_x} - \delta \tag{6}$$

$$\alpha_r = \beta - \frac{l_r r}{V_x} \tag{7}$$

The nonlinear relationship between the tire cornering force and the slip angle is shown in Fig. 2.

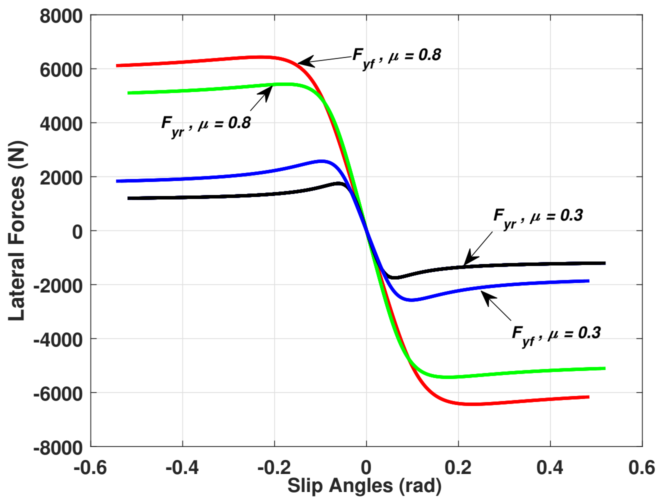

Fig. 2. Lateral forces Vs. tire slip angles

Table 1. Coefficients of tire model

Tire	Friction Coefficient (μ)	B	C	D	E
Front	$\mu = 0.3$	11.275	1.56	-2574.7	-1.9990
Rear	$\mu = 0.3$	18.631	1.56	-1749.7	-1.7908

Equations (3) and (4) are represented in (1) by utilizing the (5), and are defined in (11) and (12):

$$\dot{\beta} = \frac{F_{yf}cos(\delta) + F_{yr}}{mV_x} - r \tag{8}$$

$$\dot{r} = \frac{l_fF_{yf}cos(\delta) - l_rF_{yr}}{I_z} \tag{9}$$

Vol. 4, No. 2, 2024, pp. 727-745

Equations (11) and (12), are utilized to find the equilibrium points and for the stability analysis.

2.2. Equilibrium Points

For the phase trajectories of the states $x_1(\beta), x_2(r)$ plane, (11) and (12) are rewritten in a compact matrix form in (10) as:

$$\begin{bmatrix} \dot{x_1} \\ \dot{x_2} \end{bmatrix} = \begin{bmatrix} f_1(x_1, x_2, u) \\ f_2(x_1, x_2, u) \end{bmatrix} \tag{10}$$

where,

$$f_1 = \dot{\beta} = \frac{F_{yf} cos(\delta) + F_{yr}}{mV_x} - r \tag{11}$$

$$f_2 = \dot{r} = \frac{l_f F_{yf} cos(\delta) - l_r F_{yr}}{I_z} \tag{12}$$

The values of phase are represented by x and the velocity vector at that point is represented by $\dot{x}$. Equation (10) is written in the form mentioned in (13) as:

$$\begin{bmatrix} \dot{x_1} \\ \dot{x_2} \end{bmatrix} = \begin{bmatrix} f_1(x_1, x_2, u) \\ f_2(x_1, x_2, u) \end{bmatrix} = \begin{bmatrix} 0 \\ 0 \end{bmatrix} \tag{13}$$

Equation (13) is solved to get the values of x_1^* and x_2^*. The obtained values are the equilibrium point (x_1^*, x_2^*) of the vehicle model is defined as the point at which the rate of change of the state variable is zero. It may also be defined as a steady state condition at which the system states does not change.

2.3. Phase Plane Analysis

The movement of the points (values of state variables) on the 2 dimensional (2D) plot of state variables generates the phase trajectory. This plot is known as phase plane plot. The 2 dimensional phase plot is limited to the selection of 2 states of the vehicle. To observe the stability of lateral dynamics, generally the yaw rate r and sideslip angle β are plotted as the 2D planes. The trajectories show the transitions of the different values of the states obtained. Theses trajectories on the plane may converge towards or diverge away from equilibrium point. The equilibrium points are stable or unstable depending on whether the trajectories are converging and diverging nature respectively.

The local stability of the nonlinear system is defined by linearising the model. Linearisation is done by calculating a square matrix known as Jacobian matrix. The Jacobian matrix of the nonlinear system is calculated at the equilibrium points. The above Jacobian matrix is calculated at the equilibrium point (x_1^*, x_2^*) to obtain the eigenvalues. Equation (14) describes the Jacobian matrix as:

$$J = \begin{bmatrix} \frac{\partial f_1}{\partial x_1} & \frac{\partial f_1}{\partial x_2} \\ \frac{\partial f_2}{\partial x_1} & \frac{\partial f_2}{\partial x_2} \end{bmatrix} \tag{14}$$

The matrix J obtained at (x_1^*, x_2^*) is the constant matrix. By applying the characteristics equation $|J - \lambda I| = 0$, two roots λ_1, λ_2 are obtained. These roots are the eigenvalues of (x_1^*, x_2^*). If the eigenvalues obtained are negative, then the equilibrium points are stable and if the eigenvalues are positive then the equilibrium points are unstable.

2.4. Bifurcation Theory

The topological structure of the phase plane obtained varies with the change in the control parameters under consideration. Particularly, the equilibrium point will appear or disappear, thus resulting in a change in the stability of the system. The phenomenon of qualitative change in dynamics is known as bifurcation. The point at which stability changes is called a bifurcation point. To analyze the type of bifurcation exists in the nonlinear model, the variation in the control parameter is done.

A Hopf bifurcation (HB) is encountered when there is variation in the control parameter, the generated complex conjugate eigenvalue crosses the imaginary axis and enters into the right half of the complex plain [43]. The sign of the real part of the eigenvalue changes from negative to positive. The type of HB is either supercritical or subcritical depending on how the limit cycle interacts with the equilibrium point. The presence of unstable limit cycles prior to the bifurcation (inside the stable region) makes it subcritical. When the unstable limit cycle emerges from the subcritical Hopf point, the system becomes unstable because perturbations with larger amplitudes than the amplitude of the unstable limit cycle grows. The unstable limit cycle repels the small perturbation, while the stable fixed point attracts it. Therefore, a subcritical bifurcation is hard and dangerous in nature. If the limit cycle is stable in the unstable region after the bifurcation is supercritical. Further, if the First Lyapnouv Coefficient (FLC) is positive, then it is a subcritical Hopf and for negative it is a supercritical Hopf bifurcation [44], [45].

Bifurcation analysis plays a vital role in the nonlinear vehicle dynamics to assess the stable region of driving. The presence of bifurcations in the vehicle models results in the instability of the vehicle. The vehicle instability is caused by a saddle point. This is a point is an unstable equilibrium point. A vehicle in straight ahead running can cause the bifurcation when speed exceeds the limit speed, which can lead to vehicle instability bifurcation [46], [47]. Using multibody dynamics simulation software that enables to use the highly nonlinear dynamic elements, stable and saddle equilibrium points are shown between the β and wheel angular velocity ω. A spinning behaviour of the vehicle occurs if only a unstable equilibrium point exists for the set of bifurcation parameter value and can be mathematically analysed as a saddle node bifurcation [48]. The vehicle speed, tire-road friction condition, and steering angle varies the saddle points in the phase plane [11].

3. Simulation Results and Discussions

The values of the parameters utilized for the simulation purpose is listed in Table 2. Utilizing the MATLAB/Simulink platform, the phase trajectories plot of the lateral dynamics model for different initial conditions are obtained. The vehicle dynamics while driving change dynamically on slippery or wet surfaces for higher steering angle and longitudinal velocity. This may lead the vehicle into a region of instability. Therefore, a driving stability region must be defined for a given set of vehicle parameters for control and stability.

Table 2. Vehicle parameters

Vehicle Paramters	Values
Mass (m)	1650 kg
Distance of CG from Front Axle l_f	1.16 m
Distance of CG from Rear Axle l_r	1.9 m
Yaw Moment of Inertia I_z	2280 kg/m^2

This paper focuses on the study of a 2 DOF nonlinear vehicle model travelling with a combination of different longitudinal velocities on low friction coefficient roads for a wide range of steering angles (± 0.2 rad.). Considering the assumptions made to develop the bicycle model, the stability analysis of the model is confined to the lateral dynamics in this paper. Without these assumptions more number of dynamics can be included in modelling. Doing so, the phase plane analysis can be done between lateral, longitudinal, yaw and vertical dynamics. The behaviour of the vehicle for clockwise and anti-clockwise rotation of the steering is similar with a difference of polarity. The anti-clockwise rotation of steering is taken as a negative value. The objective is to anaylze the stability behaviour of a nonlinear vehicle model utilizing phase plane and bifurcation analysis. For the purpose of simulation, the road friction coefficient is taken as a low constant value rather than a continuous changing variable. Similarly, the values of vehicle parameters are taken as a constant values which may vary in a real vehicle. The validation of the assumptions made while developing model for simulation can be performed by utilizing the vehicle simulators including Carsim.

3.1. Phase Trajectories Analysis

Phase space analysis is utilized to show the equilibrium point bifurcation characteristics for the control parameters opted as steering angle and longitudinal velocity. The phase trajectory between $(\beta - r)$ plane for low friction coefficient is drawn in MATLAB for different combinations of steering angle and longitudinal velocity. In Fig. 3a, the phase trajectories are drawn for V_x = 10 m/s and for different $\delta = -0.02, -0.06, -0.09$ rads. The trajectories are repelled away from an unstable equilibrium point depicted by the red dot. The point at which the trajectories are attracted is represented by a green dot, thus it is a stable equilibrium point. The presence of a stable equilibrium represents that, the model will converge to the specific values of state even after disturbance. The system has three equilibrium points for the given set of parameters, out of which one is a stable equilibrium (stable node) point at $[-0.0001, -0.057]$ with a negative eigenvalue and two others are unstable equilibrium points (saddle) at $[-0.095, 0.215]$, $[-0.065, -0.225]$.

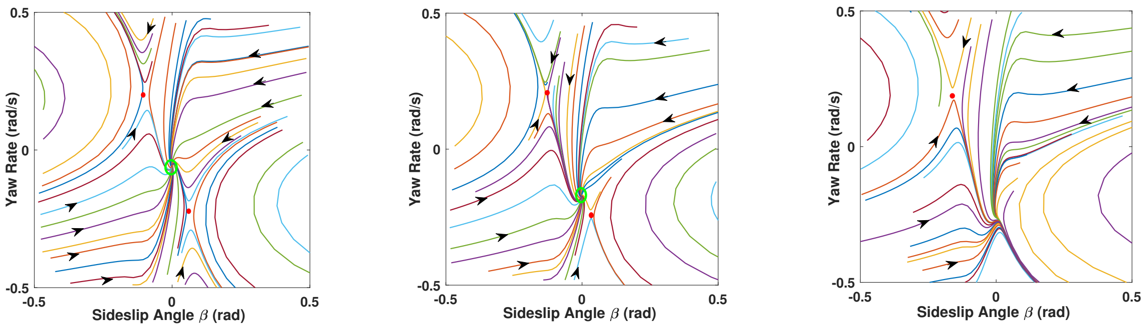

(a) $\delta = -0.02$ **(b)** $\delta = -0.06$ **(c)** $\delta = -0.09$

Fig. 3. Phase trajectories at different steering angles for $\mu = 0.3, V_x = 10m/s$

When the steering angle is changed from $\delta = -0.02$ rad to -0.09 rad, the stable and unstable equilibrium points moved towards each other and disappears. From the Figs. 3b and 3c, it can be found that, for less velocity, the disappearance of saddle and node occurs at $\delta = -0.09$. When the longitudinal velocity is increased to 20 m/s and the steering angle $\delta = -0.02$, it is found that the stable node at $[0.0154, -0.0714]$ and saddle point at $[0.06, -0.14]$ comes closer, which can be observed after comparing Figs. 3a and 4a. A further increase in steering angle, there is the disappearance of saddle and node as seen in the Fig. 4b. In Fig. 4c, the existence of an unstable limit cycle is found at steering angle $\delta = -0.12$ rad. When the V_x is increased to 30 m/s and 40 m/s, it is found that the saddle and node point becomes more closer at δ = -0.02 rad. and -0.01 rad. as depicted in Figs. 5a and 6a respectivley. Figs. 5b and 6b show that the saddle and node points are already been disappeared. A further increase in δ = -0.11 rad. at V_x= 30 m/s and V_x = 40 m/s, it is seen that the trajectories are diverging away representing an unstable limit cycle as shown in Figs. 5c and 6c. Table 3 shows the trajectory appearances for different combinations of control parameters. From the stable it is seen that, saddle and node points disappears at lower steering angle as the longitudinal velocity increases.

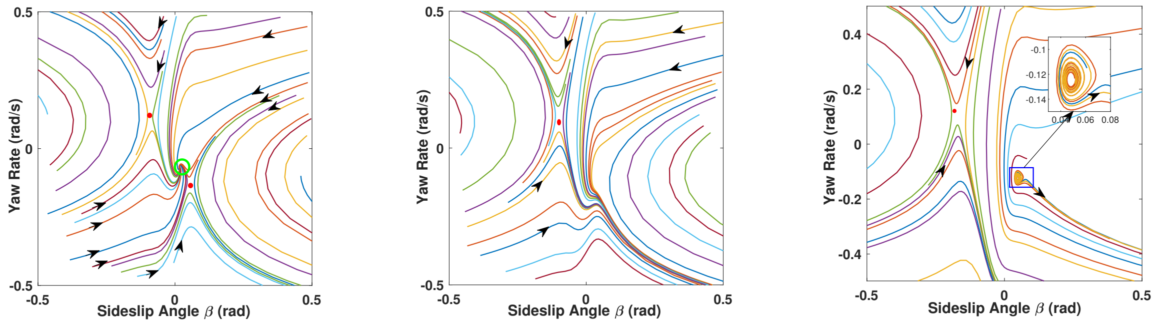

(a) $\delta = -0.02$ **(b)** $\delta = -0.06$ **(c)** $\delta = -0.12$

Fig. 4. Phase trajectories at different steering angles for $\mu = 0.3, V_x = 20m/s$

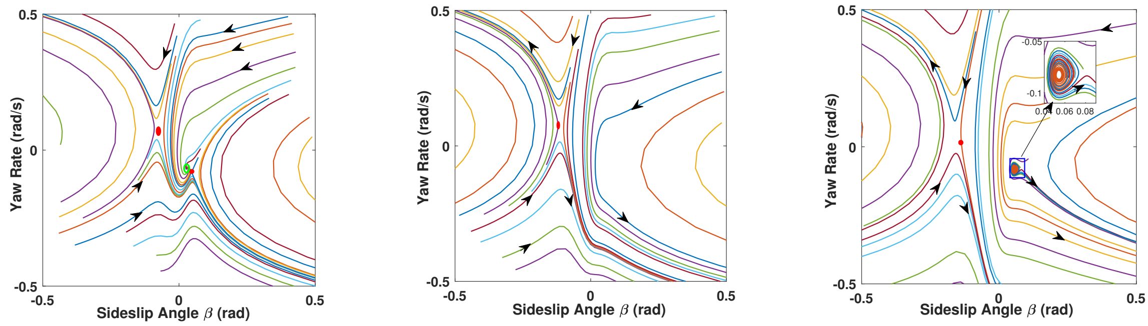

(a) $\delta = -0.02$ **(b)** $\delta = -0.06$ **(c)** $\delta = -0.11$

Fig. 5. Phase trajectories at different steering angles for $\mu = 0.3, V_x = 30m/s$

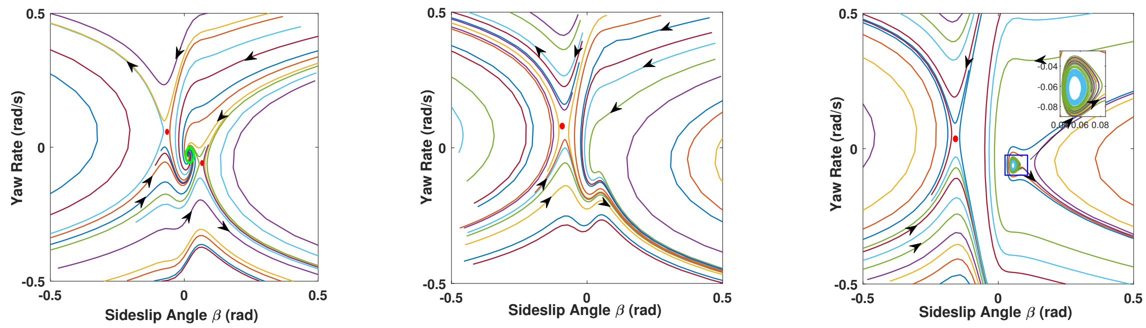

(a) $\delta = -0.01$ **(b)** $\delta = -0.02$ **(c)** $\delta = -0.11$

Fig. 6. Phase trajectories at different steering angles for $\mu = 0.3, V_x = 40m/s$

3.2. Bifurcation Analysis

For the bifurcation analysis, Matcont/Matlab is utilized to observe the type of bifurcation exists in the model based on the change in the bifurcation parameter. Matcont is a graphical Matlab software package. It is utilized to find the equilibrium states, limit points, Hopf points, limit cycles, and fold bifurcation points of limit cycles. Following are the steps involved to plot the bifurcation diagrams in Matcont.

- To utilize the Matcont, the file directory of the Matcont folder must be selected in the command window.
- In the Matcont window, choose select >> system >> New.

Vol. 4, No. 2, 2024, pp. 727-745

Table 3. Movement of equilibrium points

V_x (m/s)	δ (rad)	Trajectories Appearance
	-0.02	St. and Unst. Eq. Pts. Appear
10	-0.06	St. and Unst. Eq. Pts. Moved Near
	-0.09	St. and Unst. Eq. Pts. Disappears
	-0.02	St. and Unst. Eq. Pts. Appears Near
20	-0.06	St. and Unst. Eq. Pts. Disappears
	-0.12	Spiral Out
	-0.02	St. and Unst. Eq. Pts. Appear
30	-0.06	St. and Unst. Eq. Pts. Disappears
	-0.11	Spiral Out
	-0.01	St. and Unst. Eq. Pts. Appears
40	-0.02	St. and Unst. Eq. Pts. Disappears
	-0.09	Spiral Out

St. and Unst. Eq. Pts.: Stable and Unstable Equilibrium Points respectively

- Define name, coordinates as yaw rate and sideslip angle, parameters involved in the modelling. Then declare the model equations in the space provided.
- After the system name is loaded, choose Type >> initial point >> point. In the starter window, enter any random values of the coordinates.
- Goto window >> graphic 2D plot >> change Abscissa to time and ordinate to one of the coordinates.
- To obtain equilibrium point Choose the Select >> Initial point >> Last point.
- To select the last point as equilibrium point choose Type >> Initial point >> Equilibrium .
- Select the parameter to be the bifurcation parameter in the starter window.
- Change the Abscissa in the plot window to the selected bifurcation parameter.
- In the numeric window, select window >> layout >> eigenvalues.
- Select compute to observe the trajectory in the 2D plot window and the respective eigenvalues in the numeric window.
- The plot will start from the equilibrium point of the ordinate and pause at the limit point (LP). Before the LP the real part of the eigenvalues is negative. At the LP the real part of the eigenvalues is zero and after resuming the plot, the real part of the eigenvalues becomes positive. The LP point denotes the bifurcation point.

For the low friction coefficient or wet surface road conditions, different combinations of steering angle and longitudinal velocity are chosen as initial points to analyze the nature of bifurcation that exists in the vehicle during motion. The bifurcation diagrams of the vehicle lateral dynamics for the front steering angle and longitudinal velocity are obtained for the different equilibrium points. The bifurcation diagrams with respect to steering angle and longitudinal velocity as bifurcation parameters are obtained in Matcont and shown in Figs. 7 and 8 respectively. As in both Figs. there are presence of limit points, so it denotes that the model has undergone a saddle node bifurcation. The solid line represents the stable region as the eigenvalues of the states are negative for the specific range of steering angle. The dashed line represents the unstable region because the eigenvalues becomes positive. Figs. 7a and 7b show the bifurcation diagrams of the sideslip angle and yaw rate with respect to the steering angle at different initial points of longitudinal velocity. From the Figs. it is seen that, as the V_x is increased from 10 m/s to 40 m/s, the stable range of steering angle decreases. It is also observed that, the stable region of sideslip angle and yaw rate increases and decreases respectively. The bifurcation diagrams of sideslip angle and yaw rate with respect to longitudinal velocity for different initial points of steering angle are shown in Figs. 8a and 8b. From the Figs it can be seen that, as the steering angle increases, the the maximum stable longitudinal velocity and sideslip angle decreases. The stable yaw rate is less for lower steering angle and the maximum stable longitudinal velocity increases.

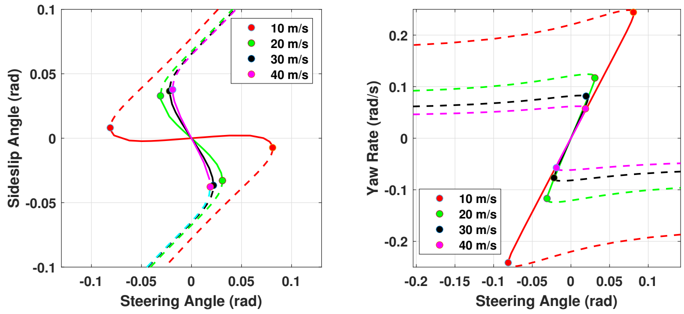

(a) β vs δ **(b)** r vs δ

Fig. 7. Saddle node bifurcation for β and r Vs δ

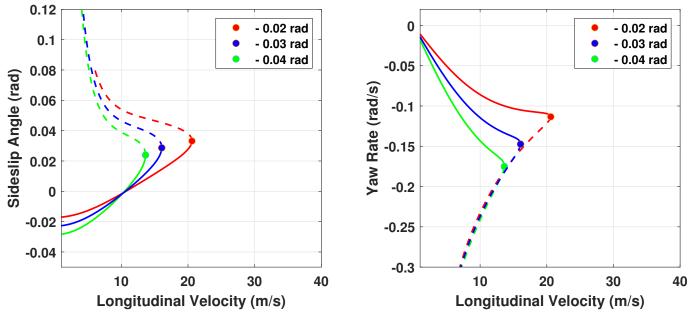

(a) β vs V_x **(b)** r vs V_x

Fig. 8. Saddle node bifurcation for β and r Vs V_x

Table 4 shows the bifurcation points of steering angles at different equilibrium points of state variables β and r considering different initial points of longitudinal velocity. The data presented in the Table 4 is obtained from Fig. 7. From the table, it can be observed that as the V_x increases, the stable range of δ bifurcation points decrease from $\pm$ 0.0812 rad. to $\pm$ 0.019 rad. Table 5 shows the bifurcation points of state variables β and r with respect to V_x. The data shown in the Table 5 is obtained from Fig. 8. It is seen that, as the steering angle increases, the bifurcation occurs at lower V_x. The maximum allowable stable longitudinal velocity decreases as δ increases. Based on the discussion, a stability region of control input parameters (bifurcation parameters) is formulated and shown in Fig. 9. This figure shows the stability region for the saddle node bifurcation analysis.

The steering angle ranges between ± 0.08 rad. with longitudinal velocity up to 40 m/s. It can be found that the stability region of longitudinal velocity decreases with the increase in steering angle. Therefore, for a stable operation of the model, the steering angle and longitudinal velocity are inversely proportional. A point in stable region in Fig. 9 corresponds to the solid lines of sideslip angle and yaw rate represented in Figs. 7 and 8 as the eigenvalues becomes negative. Similarly, a point in the unstable region in Fig. 9 corresponds to the dashed lines of sideslip angle and yaw rate represented in Figs. 7 and 8 as the eigenvalues becomes positive.

From Figs. 4c, 5c, and 6c, it is observed that, if the steering angle is increased beyond -0.08 rad and the longitudinal velocity is increased to 20 m/s and above, a limit cycle starts to appear. This is due to the fact that the eigenvalues comprise of complex conjugate part. To analyze the type of bifurcation that exists beyond -0.08 rad, the initial value of the steering angle is set at -0.1 rad value and different longitudinal velocities starting from 20 m/s are utilized. Fig. 10 depicts the Hopf bifurcation diagram wherein, the solid line represents the stable region and the dashed line represents the unstable region

Table 4. Bifurcation points for β, r vs δ

Initial Points $V_x(m/s)$	**Equilibrium Points** (β, **r**)	**Bifurcation Points** δ **(rad.)**
10	$(-0.00214, -0.11451)$	$\pm\,0.0812$
20	$(0.0338, -0.1507)$	$\pm\,0.031$
30	$(0.0509, -0.0982)$	$\pm\,0.022$
40	$(0.0569, -0.0744)$	$\pm\,0.019$

Table 5. Bifurcation points for β, r vs V_x

Initial Points δ **(rad.)**	**Equilibrium Points** (β, **r**)	**Bifurcation Points** $V_x(m/s)$
-0.02	$(-0.00214, -0.11451)$	20.5
-0.03	$(0.0338, -0.1507)$	16
-0.04	$(0.0509, -0.0982)$	13.6

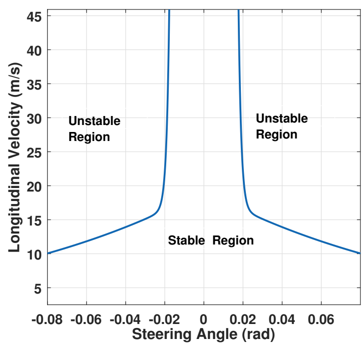

(a) V_x Vs δ

Fig. 9. Stability region of control input parameters

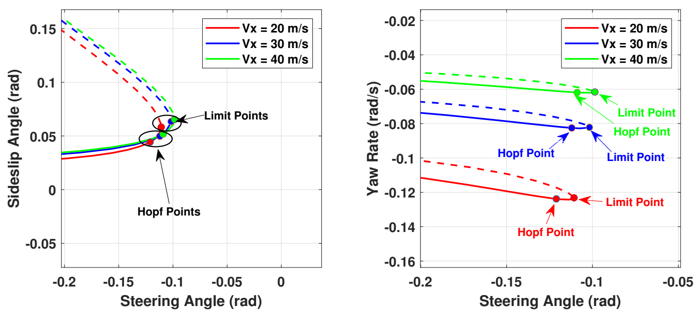

(a) β vs δ **(b)** r vs δ

Fig. 10. Hopf bifurcation for β and r Vs δ

based on the negative and positive eigenvalues obtained in the Matcont respectively. The bifurcation diagrams for sideslip angle and yaw rate with respect to steering angle at different values of V_x including 20 m/s, 30 m/s, and 40 m/s are shown in Figs. 10a and 10b. The limit point signifies the point of stability transition and Hopf point signifies the existence of Hopf bifurcation. The appearance of Hopf point prior to Limit point shows that, an unstable limit cycle exists in the stable region. The magnitude of this Limit cycle depends on the values of V_x. This existence of unstable Limit cycle is also verified by the nature of first Lyapnouv coefficient obtained in Matcont. In Matcont, the first Lyapnouv coefficients for all three velocities are obtained as $1.463e^{02}$, $9.548e^{01}$, and $7.2114e^{01}$. The obtained coefficients are positive, resulting in the presence of subcritical Hopf bifurcation. From the Table 6, it is found that, the Hopf point appeared to be in a stable region before the stability transition. As the V_x increases, the transition of stability occurs at a lower steering angle and Hopf point moves near to the bifurcation point.

Table 6. Hopf bifurcation points for β and r Vs δ

Initial Points V_x **(m/s)**	**Equilibrium Points** (β, r)	**Hopf Points** (β, r, δ)	**Bifurcation Points** δ **(rad.)**
20	(0.0609, −0.1239)	(0.0443, −0.1238, −0.121)	−0.11
30	(0.0624, −0.0831)	(0.0498, −0.0825, −0.11)	−0.101
40	(0.0608, −0.0623)	(0.0517, −0.0619, −0.10)	−0.098

The unstable limit cycles (diverging away from equilibrium point) for all three velocities are represented in Fig. 11. This unstable nature of limit cycle is generated because the equilibrium point is an unstable focus as the eigenvalues are complex conjugate with a positive real part. The increase in the magnitude of the unstable limit cycle on sideslip angle β axis more in comparison to yaw rate axis denotes that, if the V_x increases the β of the vehicle increase as shown in Figs. 11a, 11b and 11c.

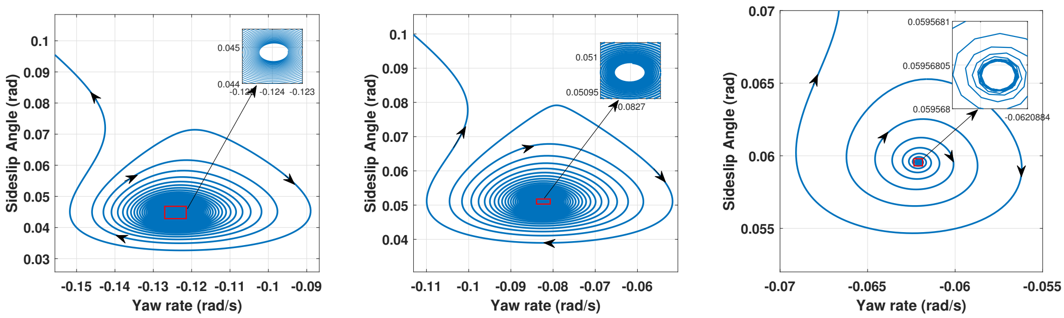

(a) For V_x = 20 m/s **(b)** For V_x = 30 m/s **(c)** For V_x = 40 m/s

Fig. 11. Unstable limit cycle

The stability region is shown in Fig. 12 for all the three velocities, where, LP represents the limit point and H represents the Hopf point. The subcritical region shown in the figure represents the existence of an unstable limit cycle. The cyan colour line bifurcates the stable and unstable region of the state variables (β, r) and the subcritical region is shown by the red dashed line. The green colour line shows the different values of sideslip angle β and yaw rate r of different values of steering angle δ and longitudinal velocity V_x. The region shown inside the red dotted line depicts the subcritical region. It can be observed that the magnitude of this region is higher in sideslip angle and lower in yaw rate. This signifies that, after the Hopf point is detected, the unstable limit cycle grows more with respect to sideslip angle of the vehicle. The magnitude of subcritical region increases on sideslip angle axis more in comparison to yaw rate axis with an increase in the value of V_x as shown in Figs. 12a, 12b and 12c.

The obtained subcritical Hopf bifurcation is also verified analytically by deriving the normal form of the vehicle model in (11) and (12). The model shows Hopf bifurcation with respect to the control parameter $\delta = -0.1$ rads. To obtain the normal form of the model, a complex number in cartesian form is introduced defined in (15).

$$v = rcos(\beta) + i(rsin(\beta)) \tag{15}$$

where,

Vol. 4, No. 2, 2024, pp. 727-745

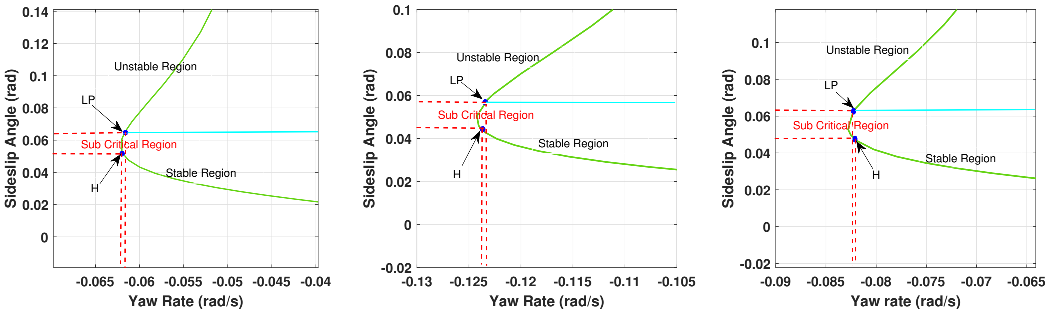

(a) V_x = 20 m/s **(b)** V_x = 30 m/s **(c)** V_x = 40 m/s

Fig. 12. Stability region

$$r = |v| \tag{16}$$

$$\beta = tan^{-1}\left\{\frac{i(\bar{v}-v)}{\bar{v}+v}\right\} \tag{17}$$

and deriving an equation for the dynamics of v. The equation is given as:

$$\frac{dv}{dt} = \left(cos(\beta)\frac{dr}{dt} - rsin(\beta)\frac{d\beta}{dt}\right) + i\left(sin(\beta)\frac{dr}{dt} + rcos(\beta)\frac{d\beta}{dt}\right) \tag{18}$$

For small angle approximation $cos(\theta) = 1, sin(\theta) = \theta$ and $tan^{-1}(\theta) = \theta$. Therefore, (18) is simplified and represented in (19).

$$\frac{dv}{dt} = \left(\frac{dr}{dt} - r\beta\frac{d\beta}{dt}\right) + i\left(\beta\frac{dr}{dt} + r\frac{d\beta}{dt}\right) \tag{19}$$

On substituting (11) and (12) in (19) and simplifying it, the equation obtained is mentioned below.

$$\begin{aligned}\frac{dv}{dt} = 23.04\delta + 18.92\beta - 5.32r + r\beta(2.82\beta - 1.37\delta + 0.93r) + i\,[\beta(23.04\delta + 18.92\beta \\ -5.32r) - r(2.89\beta - 1.37\delta + 0.93r)]\end{aligned} \tag{20}$$

Again on substituting (16) in the (20) to obtain with respect of v. The equation is defined as:

$$\begin{aligned}\frac{dv}{dt} = 23.04\delta - 5.32|v| - 2.89|v|\left[\frac{\bar{v}-v}{\bar{v}+v}\right]^2 - 1.37\delta|v|\left[\frac{i(\bar{v}-v)}{\bar{v}+v}\right] + 0.93|v|^2\left[\frac{i(\bar{v}-v)}{\bar{v}+v}\right] \\ -23.04\delta\left[\frac{\bar{v}-v}{\bar{v}+v}\right] + 5.32|v|\left[\frac{\bar{v}-v}{\bar{v}+v}\right] + 2.89|v|\left[\frac{\bar{v}-v}{\bar{v}+v}\right] + i1.37\delta|v| - i0.93|v|^2\end{aligned} \tag{21}$$

Simplifying (21), the normal formal of the Hopf bifurcation at $\delta = -0.1$ rads. for the vehicle model defined in (11) and (12) is given by following (22).

$$\begin{aligned}\frac{dv}{dt} = \left[1 - \frac{(\bar{v}-v)}{\bar{v}+v}\right][23.04 + i1.37\delta|v|] + \left[1 - \frac{(\bar{v}-v)}{\bar{v}+v}\right][-5.32|v| \\ +2.89|v|\left[\frac{i(\bar{v}-v)}{\bar{v}+v}\right] + i0.93|v|^2\Big]\end{aligned} \tag{22}$$

Equation (22) represents that the Hopf bifurcation is subcritical type as the coefficient of the $|v|^2$ is positive.

A comparison table is formulated to show the values of longitudinal velocity and steering angle utilized in the previous work to explore the type of bifurcation exists in the nonlinear model. Table 7 show the comparative analysis between the analysis performed in this paper and the work available in literature [27], [34] and [37] respectively. It can be observed that presence of saddle node and subcritical Hopf bifurcation is found for lower and higher values of control parameters respectively.

Table 7. Comparison table

V_x **(m/s)**	δ **(rad.)**	**Type of Bifurcation observed**
V_x = 10, 20, 30	upto 0.02	Saddle Node [27]
V_x = 10, 20, 30, 40	upto 0.04	Saddle Node [34]
V_x = 33	0.01	Saddle Node [37]
V_x = 10, 20, 30, 40	upto 0.11	Saddle Node and Subcritical Hopf [proposed analysis]

In the phase plane analysis, the phase trajectories are obtained for different values of steering angle and longitudinal velocity. It is observed that when the steering angle is increased from 0 rad., a saddle node bifurcation occurs. A further increase reveals that, an unstable limit cycle is present. The disappearance of saddle and node points occurs at lower values of steering angle as the longitudinal velocity increases. This implies that the saddle node bifurcation is occurring more frequently. The presence of saddle node bifurcation reveals a spinning behaviour of the vehicle that leads to the instability of the vehicle. Therefore, a saddle node bifurcation (SNB) is present for low steering angles. To analyze the nature of bifurcation that exists near the stability boundary, the value of the control parameter is increased. As the control parameters including steering angle and longitudinal velocity changes, the transition of stability of the vehicle occurs. This transition of stability is analysed with the help of bifurcation theory. If the steering angle is increased at higher longitudinal velocity, the presence of an unstable limit cycle is detected in the stable region. This results in the sliding and spinning of the vehicle. This behaviour of the vehicle show the instability as the sideslip angle increases drastically. In this paper, the road friction coefficient is considered as 0.3 representing a wet or slippery condition. The information of this friction is pre-assumed instead of estimating.

4. Conclusion

The work performed in the paper provide details about the stability analysis of a nonlinear vehicle model utilizing a phase plane and bifurcation theory for different values of steering angle and longitudinal velocity. The aim of selection of different values is to reflect the real vehicle driving scenario. It is important to know the behaviour of a vehicle on the wet road surface to avoid the accidents, therefore, a low friction coefficient is opted. The Matcont/Matlab software tool is utilized as it is much flexible to declare the mathematical equations and for the analysis of the physical models. From the stability analysis, the major findings are summarized as follows:

- For lower steering angle values ($\delta \leq \pm$ 0.8 rad) at different longitudinal velocities V_x, a saddle node bifurcation exists. This bifurcation found to be occur more frequently for higher values of longitudinal velocity as one unstable equilibrium point and stable equilibrium point moves closer to each other faster. It is found that, stability region narrows down for higher values of longitudinal velocity with lower values steering angle.
- The spin behaviour of the vehicle is found to be occur for a saddle node bifurcation (SNB) if the values of longitudinal velocity is increased on a wet surface road. This results in the yaw instability and the driver will lose control on braking the vehicle.
- For the increased values of steering angle and longitudinal velocity beyond a specific value of ($\pm$0.08 rad) and (20 m/s) respectively, a Hopf point is detected before the limit point. Based

on the Lyapnouv First Coefficient obtained in Matcont, it is observed that the Hopf bifurcation is subcritical in nature. Therefore, an unstable limit cycle is present in the stable region. The derived analytical result obtained confirms the subcritical type of Hopf bifurcation.
- The presence of unstable limit cycle in the stable region results in the increase in sideslip angle with an increase in the values of longitudinal velocity. The increase in β results in the sliding of the vehicle during cornering. It is found that, the subcritical region increases with the increase in the values of the longitudinal velocity. Therefore, for higher values of control parameters, inside the stable region, a global stability boundary exists that needs to be considered during controller design. Due to this subcritical region, the driver will lose control in steering the vehicle and will result in accident for the increased values of control parameters.

The future scope of work includes finding the global stability region inside the stable region and designing controller based on the stability region obtained. The design of bifurcation controller can eliminate the existence of SNB and the unstable limit cycle in the stable region such to control the vehicle and to avoid the accidents. The estimation techniques can be employed to provide the information about the road condition to the vehicle prior. Getting the prior information about road, the driver assistance system can be alert so that an increase steering angle and longitudinal velocity can be avoided for the vehicle and passenger safety.

Author Contribution: All authors contributed equally to the main contributor to this paper. All authors read and approved the final paper.

Acknowledgement: The authors Thank the National Institute of Technology Patna, India for providing the platform for research.

Conflicts of Interest: The authors declare no conflict of interest.

References

[1] Y. Zhu *et al.,* “A simulation study for lateral stability control of vehicles on icy asphalt pavement,” *Journal of advanced transportation*, vol. 2022, pp. 1–15, 2022, https://doi.org/10.1155/2022/7361881.

[2] R. Hajiloo, A. Khajepour, A. Kasaiezadeh, S. -K. Chen and B. Litkouhi, “Integrated Lateral and Roll Stability Control of Multi-Actuated Vehicles Using Prioritization Model Predictive Control,” in *IEEE Transactions on Vehicular Technology*, vol. 71, no. 8, pp. 8318-8329, 2022, https://doi.org/10.1109/TVT.2022.3174172.

[3] M. Ataei, A. Khajepour, and S. Jeon, “Model predictive control for integrated lateral stability, traction/braking control, and rollover prevention of electric vehicles,” *International Journal of Vehicle Mechanics and Mobility*, vol. 58, no. 1, pp. 49–73, 2020, https://doi.org/10.1080/00423114.2019.1585557.

[4] H. Liu, L. Zhang, P. Wang and H. Chen, “A Real-Time NMPC Strategy for Electric Vehicle Stability Improvement Combining Torque Vectoring With Rear-Wheel Steering,” in *IEEE Transactions on Transportation Electrification*, vol. 8, no. 3, pp. 3825-3835, 2022, https://doi.org/10.1109/TTE.2022.3153388.

[5] R. Hajiloo, A. Khajepour, A. Kasaiezadeh, S. -K. Chen and B. Litkouhi, “A Model Predictive Control of Electronic Limited Slip Differential and Differential Braking for Improving Vehicle Yaw Stability,” in *IEEE Transactions on Control Systems Technology*, vol. 31, no. 2, pp. 797-808, 2023, https://doi.org/10.1109/TCST.2022.3206282.

[6] S. H. Strogatz, *Nonlinear dynamics and chaos with student solutions manual: With applications to physics, biology, chemistry, and engineering*, CRC Press, 2018, https://doi.org/10.1201/9780429399640.

[7] M. R. Roussel, *Nonlinear Dynamics: A hands-on introductory survey*, Morgan & Claypool Publishers, 2019, https://dx.doi.org/10.1088/2053-2571/ab0281.

[8] F. Wu and Y. Jiao, “Stability and hopf bifurcation of a predator-prey model,” *Boundary Value Problems*, vol. 2019, pp. 1–11, 2019, https://doi.org/10.1186/s13661-019-1242-9.

[9] J. Wang, L. Ma, and Y. Wang, "Hopf bifurcation control for the main drive delay system of rolling mill," *Advances in Difference Equations*, vol. 2020, pp. 1–12, 2020, https://doi.org/10.1186/s13662-020-02666-1.

[10] K. E. Church *et al*., *Bifurcation theory of impulsive dynamical systems*, Springer, 2021, https://doi.org/10.1007/978-3-030-64533-5.

[11] C. E. Beal and C. Boyd, "Coupled lateral-longitudinal vehicle dynamics and control design with three-dimensional state portraits," *International Journal of Vehicle Mechanics and Mobility*, vol. 57, no. 2, pp. 286–313, 2019, https://doi.org/10.1080/00423114.2018.1467019.

[12] M. Vignati and E. Sabbioni, "A cooperative control strategy for yaw rate and sideslip angle control combining torque vectoring with rear wheel steering," *International Journal of Vehicle Mechanics and Mobility*, vol. 60, no. 5, pp. 1668–1701, 2022, https://doi.org/10.1080/00423114.2020.1869273.

[13] H. Zhang, J. Liang, H. Jiang, Y. Cai and X. Xu, "Stability Research of Distributed Drive Electric Vehicle by Adaptive Direct Yaw Moment Control," in *IEEE Access*, vol. 7, pp. 106225-106237, 2019, https://doi.org/10.1109/ACCESS.2019.2933016.

[14] J. Liu, J. Song, H. Li, and H. Huang, "Direct yaw-moment control of vehicles based on phase plane analysis," *Proceedings of the Institution of Mechanical Engineers, Part D: Journal of Automobile Engineering*, vol. 236, no. 10-11, pp. 2459–2474, 2022, https://doi.org/10.1177/09544070211052375.

[15] J. Liu, J. Song, H. Li, and H. Huang, "Direct yaw-moment control of vehicles based on phase plane analysis," *Proceedings of the Institution of Mechanical Engineers, Part D: Journal of Automobile Engineering*, vol. 236, no. 10-11, pp. 2459–2474, 2022, https://doi.org/10.1177/09544070211052375.

[16] J. Liang, J. Feng, Y. Lu, G. Yin, W. Zhuang and X. Mao, "A Direct Yaw Moment Control Framework Through Robust T-S Fuzzy Approach Considering Vehicle Stability Margin," in *IEEE/ASME Transactions on Mechatronics*, vol. 29, no. 1, pp. 166-178, 2024, https://doi.org/10.1109/TMECH.2023.3274689.

[17] N. Ahmadian, A. Khosravi, and P. Sarhadi, "Driver assistant yaw stability control via integration of afs and dyc," *Vehicle system dynamics*, vol. 60, no. 5, pp. 1742–1762, 2022, https://doi.org/10.1080/00423114.2021.1879390.

[18] J. Zhang and J. Li, "Integrated vehicle chassis control for active front steering and direct yaw moment control based on hierarchical structure," *Transactions of the Institute of Measurement and Control*, vol. 41, no. 9, pp. 2428–2440, 2019, https://doi.org/10.1177/0142331218801131.

[19] A. d. S. Mendes, A. d. T. Fleury, M. Ackermann, F. Leonardi, and R. Bortolussi, "Assessing the influence of the road-tire friction coefficient on the yaw and roll stability of articulated vehicles," *Proceedings of the Institution of Mechanical Engineers, Part D: Journal of Automobile Engineering*, vol. 233, no. 12, pp. 2987–2999, 2019, https://doi.org/10.1177/0954407018812957.

[20] Y. Huang and Y. Chen, "Vehicle Lateral Stability Control Based on Shiftable Stability Regions and Dynamic Margins," in *IEEE Transactions on Vehicular Technology*, vol. 69, no. 12, pp. 14727-14738, 2020, https://doi.org/10.1109/TVT.2020.3036780.

[21] Q. Cui, R. Ding, C. Wei, and B. Zhou, "Path-tracking and lateral stabilisation for autonomous vehicles by using the steering angle envelope," *International Journal of Vehicle Mechanics and Mobility*, vol. 59, no. 11, pp. 1672–1696, 2021, https://doi.org/10.1080/00423114.2020.1776344.

[22] S. Milani, H. Marzbani, and R. N. Jazar, "Vehicle drifting dynamics: discovery of new equilibria," *Vehicle system dynamics*, vol. 60, no. 6, pp. 1933–1958, 2022, https://doi.org/10.1080/00423114.2021.1887499.

[23] X. Zhang, P. Wang, J. Lin, H. Chen, J. Hong, and L. Zhang, "Real-time nonlinear predictive controller design for drive-by-wire vehicle lateral stability with dynamic boundary conditions," *Fundamental Research*, vol. 2, no. 1, pp. 131–143, 2022, https://doi.org/10.1016/j.fmre.2021.07.010.

[24] F. Meng, S. Shi, M. Bai, B. Zhang, Y. Li, and N. Lin, "Dissipation of energy analysis approach for vehicle plane motion stability," *Vehicle system dynamics*, vol. 60, no. 12, pp. 4035–4058, 2022, https://doi.org/10.1080/00423114.2021.1988115.

[25] I. Vörös, D. Takács, and G. Orosz, "Safe Lane-Keeping With Feedback Delay: Bifurcation Analysis and Experiments," in *IEEE Control Systems Letters*, vol. 7, pp. 1147-1152, 2023, https://doi.org/10.1109/LCSYS.2022.3231823.

[26] S. Oh, S. S. Avedisov, and G. Orosz, "On the handling of automated vehicles: modeling, bifurcation analysis, and experiments," *European Journal of Mechanics-A/Solids*, vol. 90, 2021, https://doi.org/10.1016/j.euromechsol.2021.104372.

[27] F. Lai, C. Huang, and X. Ye, "Analysis of vehicle driving stability based on longitudinal-lateral and vertical unified dynamics model," *International journal of automotive technology*, vol. 23, no. 1, pp. 73–87, 2022, https://doi.org/10.1007/s12239-022-0006-1.

[28] X. Wang and S. Shi, "Vehicle coupled bifurcation analysis of steering angle and driving torque," *Proceedings of the Institution of Mechanical Engineers, Part D: Journal of Automobile Engineering*, vol. 235, no. 7, pp. 1864–1875, 2021, https://doi.org/10.1177/0954407020985405.

[29] M. Steinherr Zazo and J. D. Rademacher, "Bifurcation control for a ship maneuvering model with non smooth nonlinearities," *arXiv:Dynamical Systems*, pp. 1–30, 2022, https://doi.org/10.48550/arXiv.2104.10663.

[30] C. G. Bobier-Tiu, C. E. Beal, J. C. Kegelman, R. Y. Hindiyeh, and J. C. Gerdes, "Vehicle control synthesis using phase portraits of planar dynamics," *Vehicle System Dynamics*, vol. 57, no. 9, pp. 1318–1337, 2019, https://doi.org/10.1080/00423114.2018.1502456.

[31] Y. Wang, S. Shi, S. Gao, Y. Xu and P. Wang, "Active Steering and Driving/Braking Coupled Control Based on Flatness Theory and a Novel Reference Calculation Method," in *IEEE Access*, vol. 7, pp. 180661-180670, 2019, https://doi.org/10.1109/ACCESS.2019.2959941.

[32] C. Jing, H. Shu, R. Shu, and Y. Song, "Integrated control of electric vehicles based on active front steering and model predictive control," *Control Engineering Practice*, vol. 121, 2022, https://doi.org/10.1016/j.conengprac.2022.105066.

[33] P. Petersik, D. Panja, and H. A. Dijkstra, "One-parametric bifurcation analysis of data-driven car- following models," *Physica D: Nonlinear Phenomena*, vol. 427, 2021, https://doi.org/10.1016/j.physd.2021.133016.

[34] F. Lai, C. Huang, and C. Jiang, "Comparative study on bifurcation and stability control of vehicle lateral dynamics," *SAE International Journal of Vehicle Dynamics, Stability, and NVH*, vol. 6, no. 1, pp. 35–52, 2021, https://doi.org/10.4271/10-06-01-0003.

[35] D. Moutevelis, J. Roldán-Pérez, M. Prodanovic, and S. Sanchez-Acevedo, "Bifurcation Analysis of Active Electrical Distribution Networks Considering Load Tap Changers and Power Converter Capacity Limits," in *IEEE Transactions on Power Electronics*, vol. 37, no. 6, pp. 7230-7246, 2022, https://doi.org/10.1109/TPEL.2022.3141234.

[36] J. Pauwelussen, "Axle characteristics and vehicle limit cycle behaviour," *International Journal of Vehicle Mechanics and Mobility*, pp. 1–19, 2024, https://doi.org/10.1080/00423114.2024.2322487.

[37] J. Zhu, S. Zhang, G. Wang, W. Zhang, and S. Zhang, "Research on vehicle stability region under critical driving situations with static bifurcation theory," *Proceedings of the Institution of Mechanical Engineers, Part D: Journal of Automobile Engineering*, vol. 235, no. 8, pp. 2072–2085, 2021, https://doi.org/10.1177/0954407021993941.

[38] R. Prakash and D. K. Dheer, "Evolutionary algorithms based model predictive control for vehicle lateral and roll motion control," *Arabian Journal for Science and Engineering*, vol. 48, no. 5, pp. 6857–6871, 2023, https://doi.org/10.1007/s13369-022-07267-6.

[39] H. Lee and S. Choi, "Development of Collision Avoidance System in Slippery Road Conditions," in *IEEE Transactions on Intelligent Transportation Systems*, vol. 23, no. 10, pp. 19544-19556, 2022, https://doi.org/10.1109/TITS.2022.3168668.

[40] G. Zhu, H. Jie, and W. Hong, "Nonlinear model predictive path tracking control for autonomous vehicles based on orthogonal collocation method," *International Journal of Control, Automation and Systems*, vol. 21, no. 1, pp. 257–270, 2023, https://doi.org/10.1007/s12555-021-0812-7.

[41] T. Gillespie, *Fundamentals of vehicle dynamics*, SAE international, 2021, https://books.google.co.id/books?id=LeybEAAAQBAJ&hl=id&source=gbsnavlinkss.

[42] T. Zhang, Y. Sun, Y. Wang, B. Li, Y. Tian and F. -Y. Wang, "A Survey of Vehicle Dynamics Modeling Methods for Autonomous Racing: Theoretical Models, Physical/Virtual Platforms, and Perspectives," in *IEEE Transactions on Intelligent Vehicles*, vol. 9, no. 3, pp. 4312-4334, 2024, https://doi.org/10.1109/TIV.2024.3351131.

[43] G. D. Agundis-Tinajero, J. C. Vasquez, and J. M. Guerrero, "Stability boundary analysis of islanded droop-based microgrids using an autonomous shooting method," *Energies*, vol. 15, no. 6, 2022, https://doi.org/10.3390/en15062120.

[44] V. Pandey and S. Singh, "Bifurcations emerging from a double hopf bifurcation for a bwr," *Progress in Nuclear Energy*, vol. 117, 2019, https://doi.org/10.1016/j.pnucene.2019.103049.

[45] V. Pandey, A. Saxena, and S. Singh, "Co-dimension two bifurcations of limit cycles starting from generalized hopf bifurcation for the dynamical system of nuclear reactors," *Progress in Nuclear Energy*, vol. 157, 2023, https://doi.org/10.1016/j.pnucene.2022.104561.

[46] G. Chen, X. Zhao, Z. Gao and M. Hua, "Dynamic Drifting Control for General Path Tracking of Autonomous Vehicles," in *IEEE Transactions on Intelligent Vehicles*, vol. 8, no. 3, pp. 2527-2537, 2023, https://doi.org/10.1109/TIV.2023.3235007.

[47] Z. Zhu, X. Tang, Y. Qin, Y. Huang and E. Hashemi, "A Survey of Lateral Stability Criterion and Control Application for Autonomous Vehicles," in *IEEE Transactions on Intelligent Transportation Systems*, vol. 24, no. 10, pp. 10382-10399, 2023, https://doi.org/10.1109/TITS.2023.3280200.

[48] D. A. Mantaras, P. Luque, and M. Alonso, "Phase plane analysis applied to non-explicit multibody vehicle models," *Multibody System Dynamics*, vol. 56, no. 2, pp. 173–188, 2022, https://doi.org/10.1007/s11044-022-09846-9.